Heterogeneous photodegradation of bisphenol A with iron oxides and oxalate in aqueous solution

F. B. Li[a, b], X. Z. Li[a, *], X. M. Li[b] and T. X. Liu[b], J. Dong[b]

[a] *Department of Civil and Structural Engineering, The Hong Kong Polytechnic University, Hong Kong, China.*

[b] *Guangdong Key Laboratory of Agricultural Environment Pollution Integrated Control, Guangdong Institute of Eco-Environment and Soil Science, Guangzhou, 510650, China.*

Abstract

To understand the degradation of endocrine disrupting chemicals (EDCs) with existence of iron oxides and polycarboxylic acids in the natural environment, the photodegradation of bisphenol A (BPA) at the interface of iron oxides under UV illumination was conducted. Four iron oxides were prepared by a hydrothermal process and then sintered at different temperatures of 65°C, 280°C, 310°C and 420°C named "IO-65", "IO-280", "IO-310", and "IO-420", respectively. The prepared iron oxides were characterized by X-ray diffraction (XRD) and Brunauer- Emmett- Teller (BET) methods. The XRD pattern of IO-65 showed a crystal structure of lepidocrocite (γ-FeOOH) and that of IO-420 demonstrated a crystal structure of hematite (α-Fe_2O_3), while IO-280 and IO-310 have the mixed crystal structures of maghemite (γ-Fe_2O_3) and hematite. The BET results revealed that the specific surface areas decreased with the increase of sintering temperature. The results demonstrated that the photodegradation of BPA depends strongly on the properties of iron oxides and oxalate, and pH. The properties of iron oxides influenced strongly the dependence of the BPA degradation on the oxalate concentration. The optimal initial concentrations of oxalate for BPA degradation under UV illumination were determined to be 2.0, 2.0, 2.4, and 2.0 mM for IO-65, IO-280, IO-310, and IO-420, respectively. The first-order kinetic constants *k* for BPA degradation under UV illumination in the presence of oxalate with the optimal initial concentration are ranked as IO-280 > IO-65 > IO-280 > IO-420. The experiments demonstrated that the optimal pH value should be in the range of 3-4. Furthermore, the dependence of BPA degradation should be also attributable to the formation of the dissolved Fe-oxalate in the solution and the adsorbed Fe-oxalate on the surface of iron oxides, and also the formation of hydrogen peroxide.

Keywords: Bisphenol A; Iron oxides; Oxalic acid; Photodegradation;

* *Corresponding author. Tel: (852) 2766 6016; Fax: (852) 2334 6389; E-mail address: cexzli@polyu.edu.hk or cefbli@soil.gd.cn (The first author)*

1. **Introduction**

Iron oxides are a kind of natural minerals and geocatalysts, widely existing in the earth's crust and also suspending in aqueous streams, aerosol, clouds, and fogs as fine particles [1]. Major iron oxides including hematite (α-Fe_2O_3), maghemite (γ-Fe_2O_3), goethite (α-FeOOH), and lepidocrocite (γ-FeOOH) show semiconductor properties with a narrow band gap of 2.0-2.3 eV and could be photoactive under solar irradiation [2]. The photocatalytic degradation of organic pollutants on the surface of iron oxides is very feasible and useful for removal of organic pollutants from contaminated soils and waters [3].

It is noticeable that iron oxides and polycarboxylic acids can form a photochemical system to conduct a photo-Fenton-like reaction with much higher quantum efficiency than that of the $Fe(OH)^{2+}$ photochemical process or photocatalytic reaction with iron oxides alone [4-6]. Since the polycarboxylic acids are also abundant in natural environment [7,8], this photochemical oxidation process can directly utilize natural matters such as iron oxides and polycarboxylic acids together with solar energy to decompose organic pollutants economically. It is meaningful to investigate the photochemical reaction in such an iron oxide-polycarboxylate complex system so as to better understand the natural transformation of organic pollutants. Among the family of polycarboxylic acids, oxalic acid is one of the most active members. In fact, the photochemistry of Fe(III)-oxalate complexes in natural aquatic environment, fog, precipitates, tropospheric aerosols and soil solutions have received considerable attention over the past three decades [9-13], because the iron oxide-oxalate exhibits strong ligand-to-metal charge absorption bands in the UV and visible region. A number of investigations focused on ferrioxalate/UV and ferrioxalate/H_2O_2/UV systems for wastewater treatment [14-17]. Since they are homogeneous photochemical reactions with artificial addition of H_2O_2, these reactions do not occur in the natural environment. In fact, the photochemical reaction of iron oxide-oxalate complexes involves both mechanisms of the homogeneous reaction in aqueous solution and also the heterogeneous reaction on the surface of iron oxide [18-20], which highly relies on the characteristics of iron oxides and oxalate content.

Bisphenol A (BPA) as the raw materials of epoxy and polycarbonate resins has been extensively used in softeners, fungicides, and similar products at about 1,700 tons annually allover the world [21]. BPA can be released into the natural environment as well as surface water during manufacturing, processing and application. Since it was detected in aquatic environment, air and soil from ppb to ppm levels [21], BPA as one of endocrine disrupting chemicals has been paid great attention to its removal and degradation. Even though many literatures had reported the photocatalytic degradation of BPA by using TiO_2, TiO_2-zeolite, TiO_2 pillared montmorillonite [22-24] for wastewater treatment, to the best of our knowledge, the photocatalytic degradation of BPA in an iron oxide-oxalate complex system has been only investigated up to a limited extent. This

study was aimed at investigating the photocatalytic reaction of BPA with iron oxides and oxalate under UV illumination in order to determine the key factors affecting such a heterogeneous reaction.

2. Experimental

2.1. Preparation of iron oxides

Lepidocrocite (γ-FeOOH) samples were first prepared using ferrous chloride ($FeCl_2.4H_2O$), sodium nitrite ($NaNO_2$) and hexamethylenetetramine ($(CH_2)_6N_4$) with the following procedure [25]: 20 g of $FeCl_2.4H_2O$, 28 g of $(CH_2)_6N_4$, and 7 g of $NaNO_2$ were dissolved in 400, 80, and 80 mL of distilled water, respectively; the three solutions were well mixed to form a bluish green precipitate; the precipitate was remained in the solution and aged at 65°C for 3 h, then centrifuged and washed three times with 95% alcohol and other three times with distilled water to remove anions and organic impurities; after dried at 65°C for 48 h, the precipitate became dehydrated gel and was ground as γ-FeOOH; then the γ-FeOOH sample was sintered at 3 different temperatures of 280, 310, and 420°C for 2 h, respectively. Eventually, one non-sintered iron oxide (IO-65) and three sintered iron oxides (IO-280, IO-310, and IO-420) were obtained.

2.2. Characterization of Iron Oxides

To determine the crystal phase composition of iron oxides samples, X-ray diffraction (XRD) measurement was carried out using a Rigaku D/MAX-IIIA diffractometer with CuK_α radiation (λ = 0.15418 nm). The accelerating voltage of 35 kV and an emission current of 30 mA were applied. The specific surface area, micropore surface area, and total pore volume were measured by the Brunauer-Emmett-Teller (BET) method [26,27], in which the N_2 adsorption at -196°C was applied and a Carlo Erba Sorptometer was used.

2.3. Experimental setup and procedures

A Pyrex cylindrical photoreactor with an effective volume of 250 mL was used to conduct all photocatalytic reaction experiments, in which an 8-W UV lamp (Luzchem Research, Inc.) with the main emission at 365 nm is positioned at the centre of the vessel as a UV light source. Light intensity (I = 1.2 mW cm^{-2}) was determined using a black-ray ultraviolet meter (Model No J221). This cylindrical photoreactor is surrounded by a circulating water jacket to control temperature at 25±2 °C during the reaction, and is covered with aluminium foil to keep away from any indoor light irradiation. The BPA chemical was purchased from Aldrich. The reaction suspension was prepared by adding 0.25 g of iron oxide powder into 250 mL of BPA solution or a mixture solution of BPA and oxalic acid. Prior to photoreaction, the suspension was magnetically stirred in the dark for 30 min to establish an adsorption/ desorption equilibrium status. During the photoreaction, the aqueous

suspension was irradiated by UV light with constant aeration. During each experiment, several analytical samples were taken from the suspension at the given time intervals for analyses after centrifuged for 20 min and filtered through a 0.45 μm Millipore filter to remove the particles.

2.4. Analytical methods

The BPA concentration was determined by liquid chromatography (Finnigan LCQ DUO) with a UV detector. While a Pinnacle II C18 column (5 μm beads, 250 × 4.6 mm ID) and a mobile phase (70% HCN: 30% water) at a flow rate of 0.8 mL min^{-1} were used for BPA separation, a maximum absorption wavelength at 278 nm was used for BPA determination. The oxalic acid concentration was determined by ion chromatography (Dionex DX-120), in which an ion column (IONPAC ASII-AC) together with a guard column (AGII-HC 4 mm) was used and a mobile phase consisting of 15 mM KOH solution was operated at a flow rate of 1.5 mL min^{-1}. Total Fe concentration was analysed by atomic absorption spectrometry and ferrous ion (Fe^{2+}) concentration was analyzed by the ferrozine method. In this study, the adsorbed $Fe^{3+/2+}$ species and Fe^{2+} species on the surface of iron oxides were extracted by using 0.1 mol L^{-1} HCl solution under 30 min stirring prior to the above analyses. The H_2O_2 concentration in the solution was determined using a H_2O_2-photometer (Lovibond ET-8600 Germany) at LED 528 nm with a detection limit of 0.03 mg L^{-1}.

3. Results and Discussion

3.1. Crystal structure and physical properties of iron oxides

The prepared 4 iron oxide samples were first examined by XRD to determine their crystal structure. The XRD patterns as shown in Fig. 1 confirmed that the IO-65 sample has 8 characteristic peaks of (020), (120), (031), (111), (051), (220), (151), and (231), attributable to lepidocrocite, and the IO-420 sample has other 8 characteristic peaks of (012), (104), (110), (113), (024), (116), (214), and (300), attributable to hematite. Furthermore, the XRD results showed that the IO-280 and IO-310 samples contain some characteristic peaks, attributable to both of maghemite and hematite. It can be seen that IO-280 has a broad peak at 2θ = 35.7° representing a maghemite peak of (311) and also a hematite peak of (110); IO-310 has a less broad peak at the same position, indicating a reduced fraction of maghemite; and IO-420 has a sharp peak at the similar position representing hematite only. These results indicate that the thermal treatment of γ-FeOOH samples achieved a phase transfer from lepidocrocite to maghemite and further to hematite. It is obvious that the content of hematite indicated by two main peaks of (104) with a d_{hkl}-value of 2.69 and (110) with a d_{hkl}-value of 2.51 in the iron oxides increases with the increased sintering temperature in this study. Unfortunately, the exact fraction of maghemite/hematite can not be determined from these limited

results. The crystal sizes of IO-65, IO-280, IO-310, and IO-420 were 13.7, 23.2, 32.6, and 54.7 nm deduced from Sherrer's formula with their strongest peak of XRD based on Fig. 1

[Fig. 1]

To investigate the pore structure and adsorption property of iron oxides, a set of nitrogen adsorption/desorption tests was carried out and their results are presented in Fig. 2. The results showed that the isotherms of iron oxides had a typical shape of Type IV curves [26], and the wide hysteresis loops of IO-65 exhibited a typical pattern of Type H2 at a relative pressure from about 0.4 to 1 while the width of hysteresis loops became narrow gradually with the increase of sintering temperature a typical pattern of Type H3 at a relative pressure from about 0.70-1, 0.75-1 and 0.86-1 for IO-280, IO-310, and IO-420, respectively. The above results indicated that iron oxides might have a porous structure [27]. The results also showed that iron oxides had mainly a disordered-porous structure and their pore volume varied against the pore size in the main range of 2-110 nm with different maximum portions at about 5, 11, 16, and 25 nm for Io-65, IO-280, IO-310, IO-420, respectively. Obviously, the pore size increased significantly with the increased temperature. The specific surface area and total pore volume of iron oxide samples were measured by the BET method. The specific surface areas of IO-65, IO-280, IO-310, and IO-420 were found to be 115.44, 75.91, 60.48 and 29.40 $m^2\ g^{-1}$, respectively, while their total pore volumes were 0.2977, 0.3485, 0.3762 and 0.2747 $m^3\ g^{-1}$, respectively. These results show that the specific surface area of the iron oxides decreases with the increased sintering temperature. However, it seems that the total pore volume does not follow the same pattern of surface area, in which the IO-310 sample has the highest total pore volume among all samples.

[Fig. 2]

3.2 Photodegradation of BPA under different reaction conditions.

Fig. 3 showed BPA degradation with an initial concentration (C_{BPA}) of 0.11 mM under the different reaction conditions. Without UV light (dark) and only with 1.2 mM oxalic acid and 1.0 g L^{-1} IO-310, the BPA concentration was only slightly decreased by 2.7% because of adsorption on the surface of iron oxide (curve a). Under UV illumination without iron oxide and oxalic acid, the removal percentage of BPA was about 3.3% after 60 min (curve b). Under UV illumination with 1.0 g L^{-1} IO-310 and without oxalic acid, the removal percentage of BPA was 23.7% after 60 min and its first-order kinetic constants was determined to be 0.45×10^{-2} min^{-1} (R^2=0.993) (curve c). When both 1.2 mM oxalic acid and 1.0 g L^{-1} iron oxide were added into the BPA solution to form the

photo-Fenton-like system under UV illumination (curve d, e, f, g), the removal percentage of BPA was significantly increased up to 68.1%, 84.0%, 67.4%, and 60.8% after 40 min reaction, and the first-order kinetic constants *k* were determined to be 3.08×10^{-2}, 5.06×10^{-2}, 2.93×10^{-2}, and 2.58×10^{-2} min^{-1} for IO-65, IO-280, IO-310, and IO-420, respectively. Obviously, the *k* value was ranked in an order of IO-280 > IO-65 > IO-310 > IO-420. The results showed that iron oxides, oxalate, and UV light all play most important roles in the BPA degradation reaction. The BPA photodegradation should be greatly enhanced in the cooperation of iron oxide and oxalate, and also strongly depended on the properties of iron oxides. The photochemical process in the presence of iron oxide and oxalate together has been described in detail [5, 6, 10, 13]. In this suspension, oxalic acid is first adsorbed on the surface of iron oxide to form iron oxide-oxalate complexes of $[\equiv Fe^{III}(C_2O_4)_n]^{3-2n}$, which can be excited to form a series of radicals including oxalate radical $(C_2O_4)^{\bullet-}$, carbon-centered radical $(CO_2)^{\bullet-}$, superoxide ion ($O_2^{\bullet-}$), •OOH and hydroxyl radical (•OH), and form H_2O_2. And Fe-oxalate complexes of $[Fe^{III}(C_2O_4)_n]^{3-2n}$ can form in the solution. It must be noted that this photochemical process happened both on the surface of iron oxide as a heterogeneous reaction and in the solution as a homogeneous reaction. To compare the efficiency in iron oxide-oxalate system with that in Fe(III)-oxalate homogeneous system, a homogeneous system was set up by adding 0.75 mM Fe^{3+} (the same amount in IO-310 suspension) and 1.2 mM oxalate to degrade BPA under UV illumination (I = 1.2 mW cm^{-2}) and the results are shown as curve h in Fig. 3. The results showed that the BPA removal was only 58.8%, much lower than that in curve f, indicating that the degradation of BPA in aqueous iron oxide-oxalate suspension was achieved by both of reaction in the solution and also the reaction on the surface of iron oxides.

[Fig. 3]

3.3. Photodegradation of BPA with iron oxides and oxalate

As an alternative technique to the photo-Fenton reaction (Fe^{2+}/H_2O_2/UVC), ferric ion (Fe^{3+}) can also catalyze the H_2O_2 decomposition in acidic solution under UVA illumination to form hydroperoxyl radicals (HO_2•) and hydroxyl radicals (•OH) known as the photo-Fenton-like reaction (Fe^{3+}/H_2O_2/UVA). Since iron oxide and oxalate can form an iron oxide-oxalate complex to enhance the photo-Fenton-like reaction [4-6], the effect of oxalic acid on BPA photodegradation becomes very interesting. Four sets of experiments under UV illumination with an initial BPA concentration of 0.11 mM and an iron oxide dosage of 1.0 g L^{-1} were carried out using IO-65, IO-280, IO-310, and IO-420, respectively. In each set of experiments, the different initial concentrations of oxalic acid (C_{ox}) up to 4.4 mM were applied. The experiments demonstrated that IO-280 achieved the best performance of BPA degradation and the results with different C_{ox} are shown in Fig. 4. The

experimental data were also fitted using the first-order kinetic model to determine its kinetic constant (k) at different C_{ox}, as showed in Fig. 5. It can be seen clearly that the BPA degradation strongly depended on C_{ox} in the 4 sets of experiments. The reaction rate was significantly increased with the increase of oxalate concentration at its low dosage, but was slightly inhibited with an excessive amount of oxalate. These results indicate that an optimal dosage of oxalate between 2.0 and 3.0 mM achieved the fastest rate of BPA degradation under these experimental conditions.

[Fig. 4]

[Fig. 5]

These experiments demonstrated clearly that the presence of iron oxides and oxalate in cooperation can greatly accelerate the BPA degradation reaction under UV illumination. The first-order kinetic constant (k) was increased 22.6 times from 2.0×10^{-3} min^{-1} without oxalate to 4.52×10^{-2} min^{-1} with oxalate for IO-65, 19.6 times for IO-280, 12.1 times for IO-310, and 11.4 times for IO-420 under UV illumination with the optimal C_{ox}. These results provide very useful information to better understand the reaction mechanism of BPA degradation in such an iron oxide-oxalate complex system. If we compare the kinetic k values under the optimized reaction conditions, the rate of BPA degradation under UV illumination can be ranked as IO-280 > IO-310 > IO-65 > IO-420.

Actually our experiments demonstrated that oxalate itself can also be degraded in such a photo-Fenton-like reaction significantly. To better understand this photocatalytic reaction, the degradation of oxalate as a side reaction was also investigated. In the above experiments, oxalate concentration was analyzed at different time intervals, and two sets of results are shown in Fig. 6. It can be seen that after 40 min reaction, oxalate was significantly degraded by nearly 80% under UV illumination. The first-order kinetic constant (k) for oxalate degradation under UV illumination was determined to be 3.73×10^{-2}, 4.18×10^{-2}, 3.62×10^{-2}, and 3.05×10^{-2} min^{-1} for IO-65, IO-280, IO-310, and IO-420, respectively. These results indicate that the degradation of oxalate depends strongly on characters of iron oxides. IO-280 achieved the highest activity for degrading oxalate under UV illumination. The kinetic constant k values for oxalate degradation under UV illumination follows the orders of IO-280 > IO-65 > IO-310 > IO-420. It should be noted that the orders of reaction rate for oxalate degradation are same as that of BPA degradation under UV illumination in such a photo-Fenton like reaction system.

[Fig. 6]

3.4 The effect of pH value on BPA photodegradation.

The pH value is also an important factor to affect such a photo-Fenton-like reaction. Two sets of experiments were conducted under UV illumination, respectively. The initial concentrations of oxalic acid and BPA were 2.4 mM and 0.11 mM, respectively. The variations of pH vs. reaction time are plotted in Fig. 7. All experiments demonstrated a rapid increase of pH especially at the early stage of reaction. It can be seen that the pH increased significantly from the initial values of 2.90, 2.90, 2.85, and 2.71 to 5.01, 5.23, 4.92, and 4.00 after 40 min reaction under UV illumination for IO-65, IO-280, IO-310, and IO-420, respectively. It is believed that the pH increase mainly resulted from the loss of oxalic acid. While IO-280 achieved the most oxalate reduction under UV illumination, they pH raised to the highest levels. A slight pH increase just prorior photoreaction was also found due to the strong adsorption of oxalate onto the surface of iron oxides in the dark. It was also noted that the order of the increased amount of pH value from high to low was in agreement with the order of the k value for oxalate degradation with 4 iron oxides.

[Fig. 7]

To investigate the effect of pH on the BPA photodegradation, a set of experiments was carried out with 1.0 g L^{-1} iron oxides in the presence of BPA (C_{BPA} = 0.11 mM) and oxalate (C_{ox} = 1.2 mM) under UV illumination. Before the reactions, pH in the solution was adjusted by adding NaOH or $HClO_4$. The experimental data at different pH values were fitted by using the first-order model and the dependence of the first-order kinetic constant *k* values on pH value was presented in Fig. 8. The results showed that BPA photodegradation should depend strongly on pH in the iron oxide-oxalate system. Obviously, there was an optimal pH value for BPA photodegradation. The maximal *k* values for different iron oxides were determined to be 3.48×10^{-2} min^{-1} at pH 3.95 for IO-65, 5.73×10^{-2} min^{-1} at pH 3.93 IO-280, 3.32×10^{-2} min^{-1} 3.93 for IO-310, and 2.73×10^{-2} at pH 3.69 for IO-420, respectively. The BPA degradation would be inhibited significantly when pH was beyond the range of about 3-4. Obviously, the pH value should be a very important factor affecting this photo-Fenton-like reaction.

Balmer and Sulzberger [13] had reported that when the pH was at around 4, the main Fe(III)-oxalate species were $Fe^{III}(C_2O_4)_2^-$ and $Fe^{III}(C_2O_4)_3^{3-}$, which are highly photoactive. In our experiment, the iron oxide-oxalate complex system at pH value of about 3-4 might have a higher concentration of $Fe^{III}(C_2O_4)_2^-$ and $Fe^{III}(C_2O_4)_3^{3-}$ in the solution, and $[\equiv Fe^{III}(C_2O_4)_2]^-$ and $[\equiv Fe^{III}(C_2O_4)_3]^{3-}$ on the surface. When the pH value increased to about 4-5, Fe(III)-oxalate species were mainly $Fe^{III}(C_2O_4)^+$ and $[\equiv Fe^{III}(C_2O_4)]^+$, which are low photoactive. When pH was up to 6, the

Fe^{3+} and Fe^{2+} almost can not exist in the solution and the predominant Fe(III) and Fe(II) species were Fe(II)-OH and Fe(III)-OH as the precipitate, which might hardly be photoactive.

[Fig. 8]

3.5. Formation of hydrogen peroxide and Fe-oxalate species

Hydrogen peroxide (H_2O_2) is an important intermediate in the aqueous iron oxides and oxalate suspension by irradiating with UV light. During the photoreaction, H_2O_2 could be formed and then decomposed by reacting with Fe^{2+} species, simultaneously. It was found in the experiments that its concentration was at a low level of below 0.3 mg L^{-1} as shown in Fig. 9. In the reaction using IO-420, the highest H_2O_2 concentration was determined to be 0.13 mg L^{-1} at 5 min reaction and then H_2O_2 concentration decreased quickly below the detection limit of 0.03 mg L^{-1} afterwards. In the other three reactions using IO-65, IO-280, IO310, and IO-420, H_2O_2 concentration varied in the range of 0.05-0.3 mg L^{-1}. These results confirmed that the H_2O_2 formation is really involved in such a photo-Fenton-like reaction, but its accumulated concentration was at a low level of blow 0.3 mg L^{-1}.

[Fig. 9]

During the photochemical reactions, some Fe-oxalate complexes of $[\equiv Fe^{III}(C_2O_4)_n]^{3-2n}$ and $[\equiv Fe^{II}(C_2O_4)_n]^{2-2n}$ on the surface of iron oxide and $[Fe^{III}(C_2O_4)_n]^{3-2n}$ and $[Fe^{II}(C_2O_4)_n]^{2-2n}$ in the solution can also be formed. The formation of Fe-oxalate species will be indispensable to the formation of hydrogen peroxide. To study the formation of Fe-oxalate species, the experiments using different catalysts (IO-65, IO-280, IO-310, and IO-420) were conducted under UV illumination with C_{ox}=1.2 mM and C_{BPA}=0.11 mM, in which dissolved Fe^{3+} and Fe^{2+} species were monitored during the BPA degradation reaction, as showed in Fig. 10A, while adsorbed $Fe^{3+/2+}$ species were showed in Fig. 10B. Fig. 10A showed that the concentration of dissolved Fe^{3+} species was much higher than that of dissolved Fe^{2+} species, and was the highest at the beginning of photoreaction and then decreased gradually along with reaction time for IO-65, IO-280 and IO-310. To be contrast, the concentration of dissolved Fe^{3+} species for IO-420 increased gradually from 0 to 30 min, and then decreased slightly. Obviously, IO-310 was dissolved at the fastest rate and IO-420 was dissolved at the slowest rate. The concentration of dissolved Fe^{2+} species increased sharply at the first few minutes of the reaction, and then either gradually reduced after a peak time for IO-65, IO-280 and IO-310, while that increased gradually along time for IO-420. It is well known that ferric ion (Fe^{3+}) can form ferric hydroxide ($Fe(OH)_3$) and well precipitate from aqueous solution in a

pH range of 5-9. It is believed that the reduction of dissolved $Fe^{2+/3+}$ species at the later stage of the reaction resulted from the precipitation of some insoluble Fe-containing compounds such as $Fe(OH)_3$ because pH jumped quickly from the initial pH below 3 up to almost 5 within the first 5 min, as shown in Fig. 7. However, the variation of adsorbed $Fe^{3+/2+}$ species was significantly different with that of dissolved $Fe^{3+/2+}$ species. Fig. 10B showed that the amount of adsorbed Fe^{3+} species on the catalyst surface had a declined trend with the increased reaction time in general, that increased at the first 5 min for IO-65 and at the first 10 min for IO-420, and then gradually decreased at the peaks, while that decreased consistently along the reaction for IO-280 and IO-310. In contrast, the amount of adsorbed Fe^{2+} species had an increased trend throughout the reaction and reached the higher levels at the later stage of reaction.

[Fig. 10]

$$[\equiv Fe^{III}(C_2O_4)_n]^{(2n-3)-} + h\nu \rightarrow Fe^{II}(C_2O_4)_2^{2-} \text{ or } \equiv Fe^{II}(C_2O_4)_2^{2-} + (C_2O_4)^{\bullet-} \quad (1)$$

$$(C_2O_4)^{\bullet-} \rightarrow CO_2 + CO_2^{\bullet-} \quad (2)$$

$$CO_2^{\bullet-} + O_2 \rightarrow CO_2 + O_2^{-\bullet} \quad (3)$$

$$\equiv Fe^{2+} + H_2O_2 \rightarrow \equiv Fe^{3+} + OH^- + \bullet OH \quad (4)$$

The experimental results showed that the formation of adsorbed $Fe^{3+/2+}$-oxalate species on the surface of IO-420 was difficult and also resulted in a low concentration of dissolved $Fe^{3+/2+}$-oxalate in the bulk solution, because of its pure composition of α-Fe_2O_3 with more stable thermodynamics than other iron oxides, which means that, the less amount of $Fe^{3+/2+}$-oxalate species led to the lower photochemical activity. It is interesting that the *k* values for oxalate degradation followed an order of IO-280 > IO-65 > IO-310 > IO-420, and the *k* values for BPA degradation in the presence of 2.4 mM oxalate followed the same order. The equations 1-3 indicate that the reaction of oxalate degradation can form oxalate radical $(C_2O_4)^{\bullet-}$, carbon-centered radical $(CO_2)^{\bullet-}$, and superoxide ion $(O_2^{\bullet-})$. Therefore, the faster oxalate degradation, implying a more effective electron transfer, may lead to the more rapid BPA degradation. In addition, the experiments in this study confirmed that the amount of adsorbed Fe^{2+}-oxalate species on the surfaces of different iron oxides in the order of IO-280 > IO-65 > IO-310 > IO-420. If it is believed that the formation of adsorbed Fe^{2+}-oxalate species on the surface of iron oxides were attributable to the electron transfer between the adsorbed Fe^{3+}-oxalate species and oxalate, the higher amount of adsorbed Fe^{2+}-oxalate species on the surface of iron oxides would imply the higher efficiency of electron transfer from oxalate. In summary, it can be seen that both the formation of adsorbed Fe^{2+}-oxalate species on the iron oxides and oxalate

degradation reaction could affect the BPA degradation reaction in an interactive way. The exact mechanism needs to be further explored in the future studies.

4. Conclusions

The experiments in this study confirmed that the iron oxides sintered at different temperatures have different crystal structures and their specific surface areas decreased with the increased sintering temperature. The BPA degradation is primarily affected by the properties of iron oxides. The existence of oxalate together with iron oxides can enhance much faster degradation of BPA in aqueous solution than iron oxides alone. It was found that the concentration of oxalate (C_{ox}) was a critical factor affecting the BPA degradation. In the meantime, oxalate degradation, pH, and the formation of hydrogen peroxide and Fe-oxalate species also play the important roles in the reaction.

Acknowledgements

The authors would thank the Research Grant Committee of Hong Kong Government for financial support to this work (RGC No: PolyU 5170/04E) and also thank China National Natural Science Foundation (Project No. 20377011) and Guangdong Natural Science Foundation (Key Project No.036533).

References

[1] U. Schwertmann, R.M. Cornell, Iron oxides in the laboratory: preparation and characterization. Second ed., WILEY-VCH, 2000.
[2] J.K. Leland, A.J. Bard, J. Phys. Chem. 91 (1981) 5076.
[3] M.A.A. Schoonen, Y. Xu, D.R. Strongin, J. Geochem. Explor. 62 (1998) 201.
[4] Y.G. Zuo, Y.W. Deng, Chemosphere 35 (1997) 2051.
[5] C. Siffert, B. Sulzberger, Langmuir 7 (1991) 1627.
[6] B.C. Faust, J. Allen, Environ. Sci. Technol. 27 (1993) 2517.
[7] B.W. Strobel, Geoderma 99 (2001) 169.
[8] J.F. Ma, S.J. Zheng, H. Matsumoto, S. Hiradate, Nature 390 (1997) 569.
[9] A. Bozzi, T. Yuranova, J. Mielczarski, A. Lopez, J. Kiwi, Chem. Commun. 19 (2002) 2202.
[10] P. Mazellier, B. Sulzberger, Environ. Sci. Technol. 35 (2001) 3314.
[11] V. Nadtochenko, J. Kiwi, J. Chem. Soc. Faraday Trans. 93 (1997) 2373.
[12] Y.G. Zuo, J. Holgné, Environ. Sci. Technol. 26 (1992) 1014.
[13] M.E. Balmer, B. Sulzberger, Environ. Sci. Technol. 33 (1999) 2418.
[14] P. Huston, J.J. Pignatello, Environ. Sci. Technol. 30 (1996) 3457.
[15] J. Jeong, J. Yoon, Water Res. 38 (2004) 3531.
[16] Y. Lee, J. Jeong, C. Lee, S. Kim, J. Yoon, Chemosphere 51 (2003) 901.
[17] X.Z. Li, M. Zhang, H. Chua, Water Sci. Technol. 33 (1996) 111-118.

[18] R.M. Smith, A.E. Martell, Critical Stability Constants; Plenum Press: New York, 1976; Vol. 2 and 3 Inorganic Complexes/Other Organic Ligands.
[19] B. Sulzberger, H. Laubscher, Mar. Chem. 50 (1995) 103.
[20] Q.G. Mulazzani, J. Phys. Chem. 90 (1986) 5347.
[21] I.T. Cousins, C.A. Staples, G.M. Klecka, D. Mackay, Hum. Ecol. Risk Assess. 8 (2002) 1107.
[22] K. Chiang, T.M Lim, L. Tsen, C.C. Lee, Appl. Catal. A: Gen. 261 (2004) 225.
[23] S. Fukahori, H. Ichiura, T. Kitaoka, H. Tanaka, Environ. Sci. Technol. 37 (2003) 1048.
[24] N. Watanabe, S. Horikoshi, H. Kawabe, Y. Sugie, J.C. Zhao, H. Hidaka, Chemosphere 52 (2003) 851.
[25] P.G. Hall, N. S. Clarke, S.C.P. Maynard, J. Phys. Chem. 99 (1995) 5666.
[26] S.L. Gregg, K.S.W. Sing, Adsorption, Surface Area and Porosity, Academic Press, London, 1982.
[27] J.G. Yu, J.C. Yu, M.K.P. Leung, W.K. Ho, B. Cheng, X.J. Zhao, J.C. Zhao, J. Catal. 217 (2003) 69.

List of Figure Captions

FIG. 1 XRD patterns of the iron oxides

FIG. 2 Pore volume distribution of iron oxides and the nitrogen adsorption-desorption isothermal curves of iron oxides at -196°C

FIG. 3 Photodegradation of 0.11 mM BPA under different conditions: (a) 1.2 mM oxalic acid + 1.0 g L^{-1} IO-310, (b) UV, (c) UV + 1.0 g L^{-1} IO-310, (d) 1.0 g L^{-1} IO-65 + UV + 1.2 mM oxalic acid, (e) 1.0 g L^{-1} IO-280 + UV + 1.2 mM oxalic acid, (f) 1.0 g L^{-1} IO-310 + UV + 1.2 mM oxalic acid, (g) 1.0 g L^{-1} IO-420 + UV + 1.2 mM oxalic acid, (h) 0.75 mM Fe^{3+} + UV + 1.2 mM oxalic acid

FIG. 4 Effect of the initial concentration of oxalic acid on the BPA degradation with the initial concentration of 0.11 mM under UV illumination by using IO-65 (A), IO-280 (B), IO-310 (C), and IO-420 (D)

FIG. 5 Dependence of the first-order kinetic constants of the BPA degradation on the initial concentration of oxalic acid under UV light illumination

FIG. 6 Dependence of the first-order kinetic constant *k* value on the pH value in the solution by using 1.0 g L^{-1} iron oxides in the presence of BPA with the initial concentration of 0.11 mM and oxalate with the initial concentration of 1.2 mM under UV light

FIG. 7 Effect of iron oxides with the dosage of 1 g L^{-1} on the photodegradation of oxalate under UV light illumination in the presence of C_{ox} = 2.4 mM and C_{BPA} = 0.11 mM

FIG. 8 Effect of iron oxides with the dosage of 1 g L^{-1} on the variation of pH under UV light illumination in the presence of C_{ox} = 2.4 mM and C_{BPA} = 0.11 mM

FIG. 9 Effect of iron oxides with the dosage of 1 g L^{-1} on the formation of peroxide hydrogen under UV light illumination in the presence of C_{ox} = 2.4 mM and C_{BPA} = 0.11 mM

Fig. 10 Concentration of dissolved Fe^{3+} and Fe^{2+} species in the solution (A) and adsorbed Fe^{3+} and Fe^{2+} species on the surface (B) plots on reaction time with C^0_{ox} = 2.4 mM and C_{BPA} = 0.11 mM under UV illumination

FIG. 1

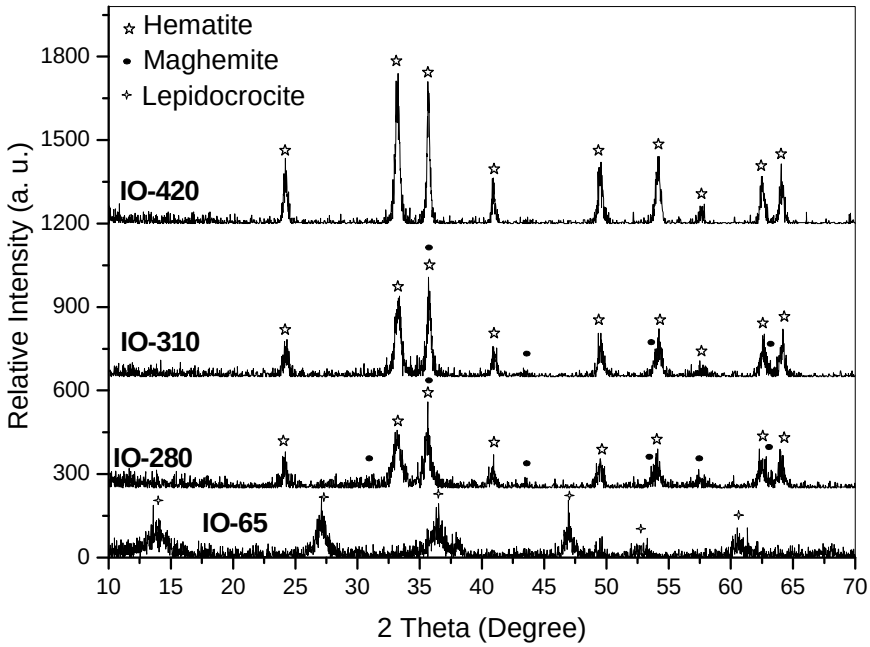
Hematite
Maghemite
Lepidocrocite
IO-420
IO-310
IO-280
IO-65
Relative Intensity (a. u.)
2 Theta (Degree)
0
300
600
900
1200
1500
1800
10
15
20
25
30
35
40
45
50
55
60
65
70

FIG. 2

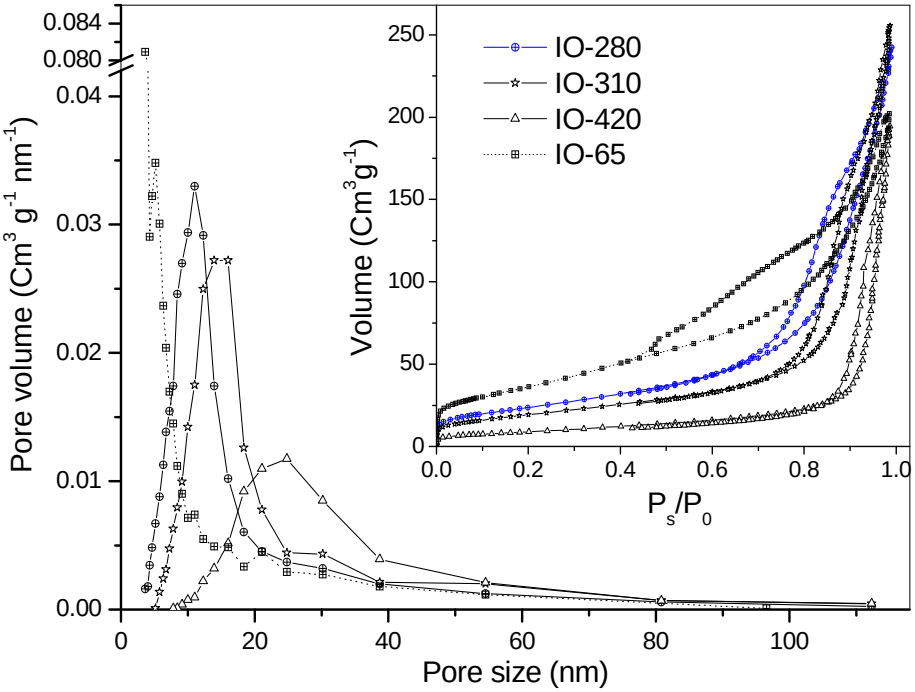
Pore volume (Cm^3 g^{-1} nm^{-1})
Pore size (nm)
0.084
0.080
0.04
0.03
0.02
0.01
0.00
0
20
40
60
80
100
Volume (Cm^{3}g^{-1})
P$_s$/P$_0$
IO-280
IO-310
IO-420
IO-65
250
200
150
100
50
0
0.0
0.2
0.4
0.6
0.8
1.0

FIG. 3

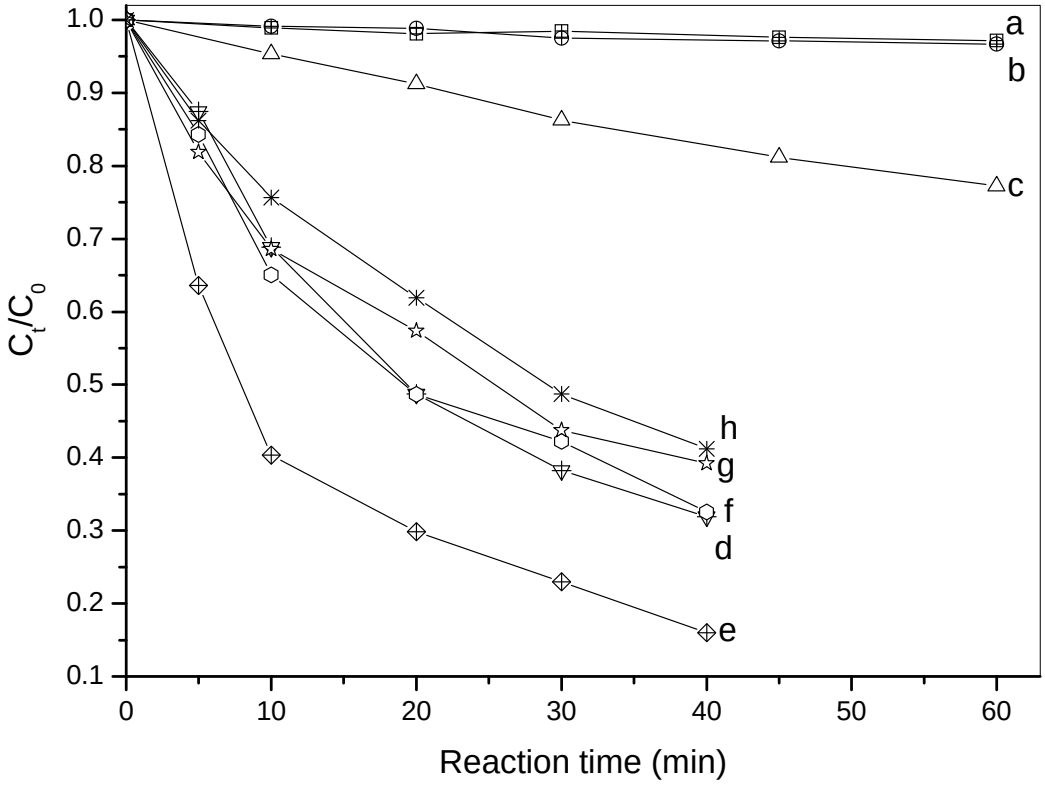
1.0
0.9
0.8
0.7
0.6
0.5
0.4
0.3
0.2
0.1
C_t/C_0
0
10
20
30
40
50
60
Reaction time (min)
a
b
c
h
g
f
d
e

FIG. 4

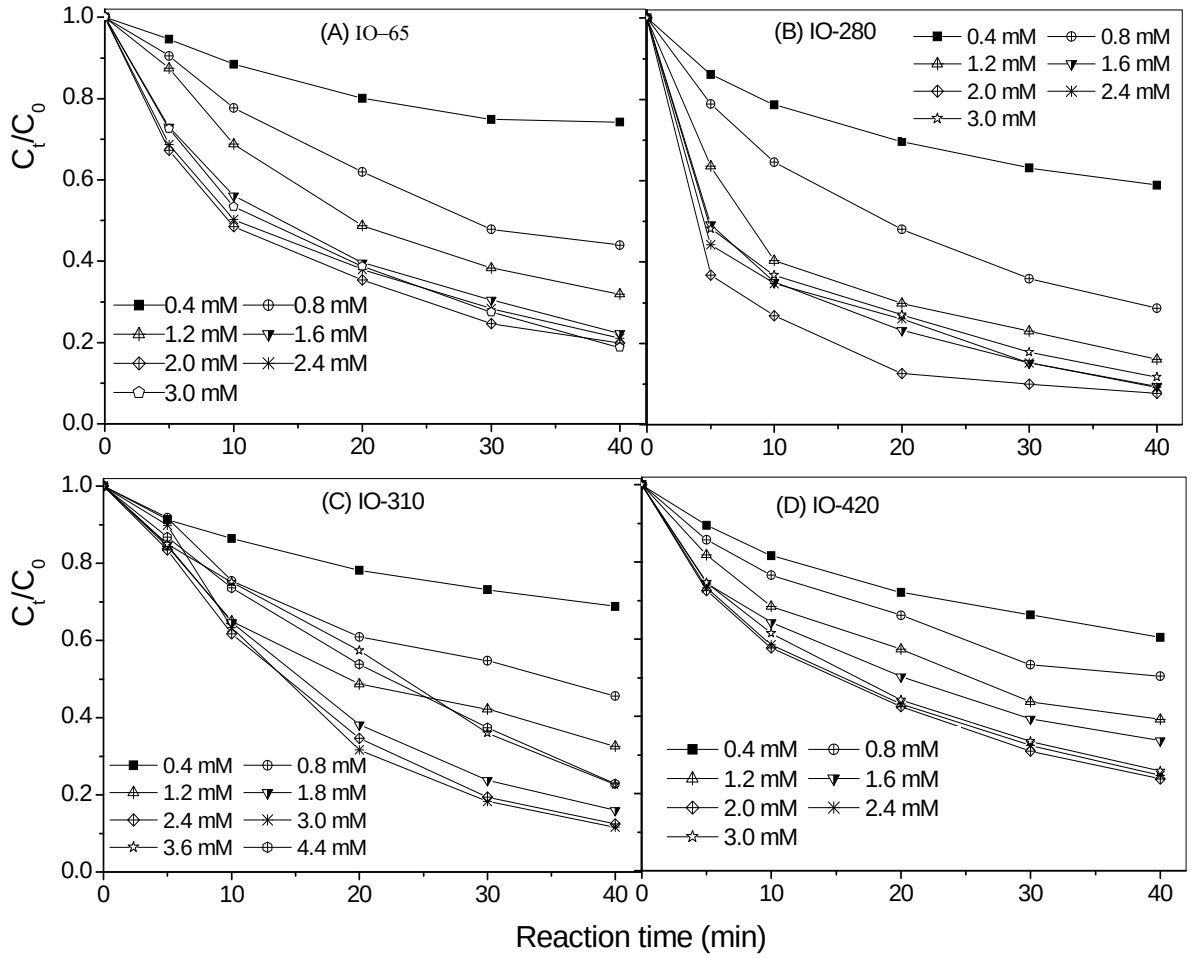
(A) IO–65
(B) IO-280
(C) IO-310
(D) IO-420
C_t/C_0
Reaction time (min)
0.4 mM
0.8 mM
1.2 mM
1.6 mM
1.8 mM
2.0 mM
2.4 mM
3.0 mM
3.6 mM
4.4 mM

FIG. 5

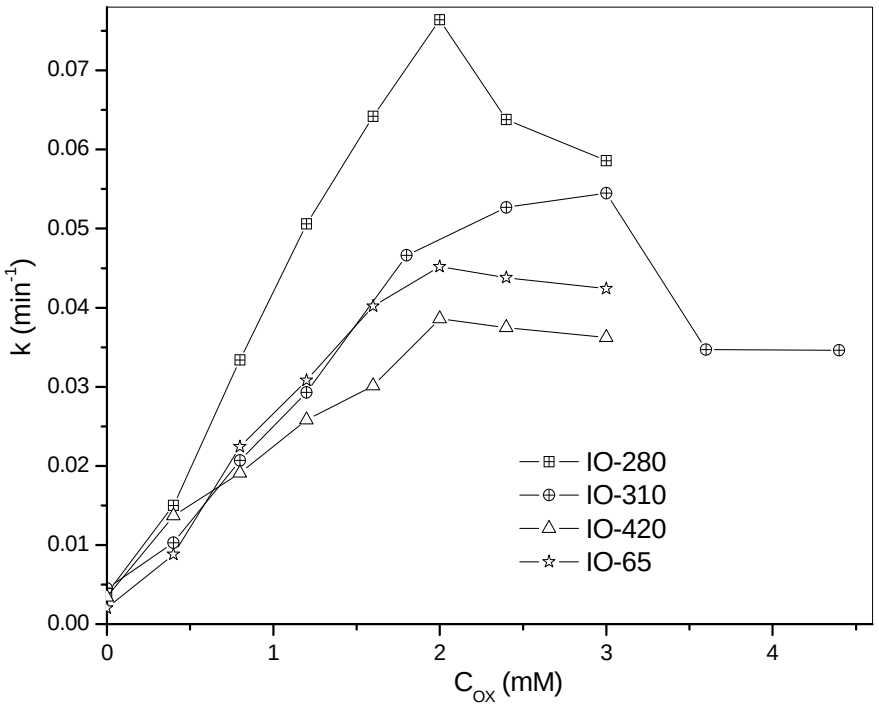
k (min-1)
0.00
0.01
0.02
0.03
0.04
0.05
0.06
0.07
0
1
2
3
4
COX (mM)
IO-280
IO-310
IO-420
IO-65

FIG. 6

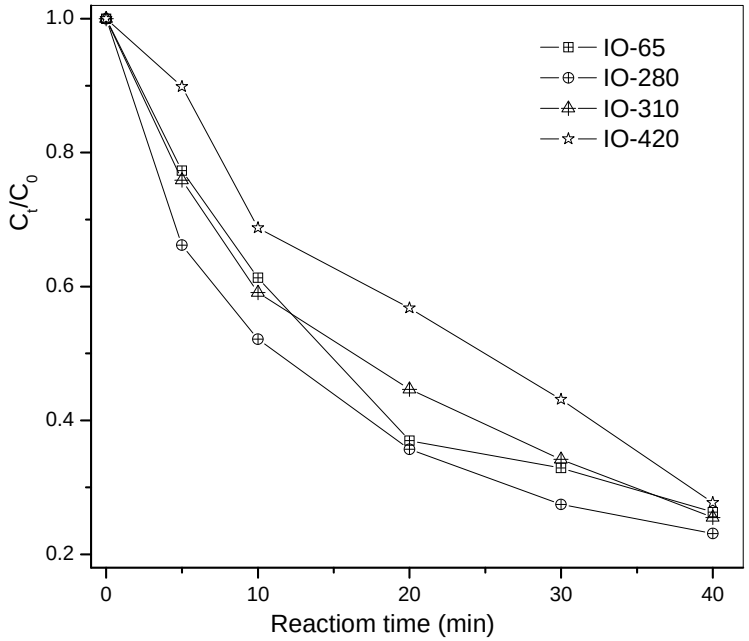
IO-65
IO-280
IO-310
IO-420
C_t/C_0
1.0
0.8
0.6
0.4
0.2
0
10
20
30
40
Reactiom time (min)

FIG.7

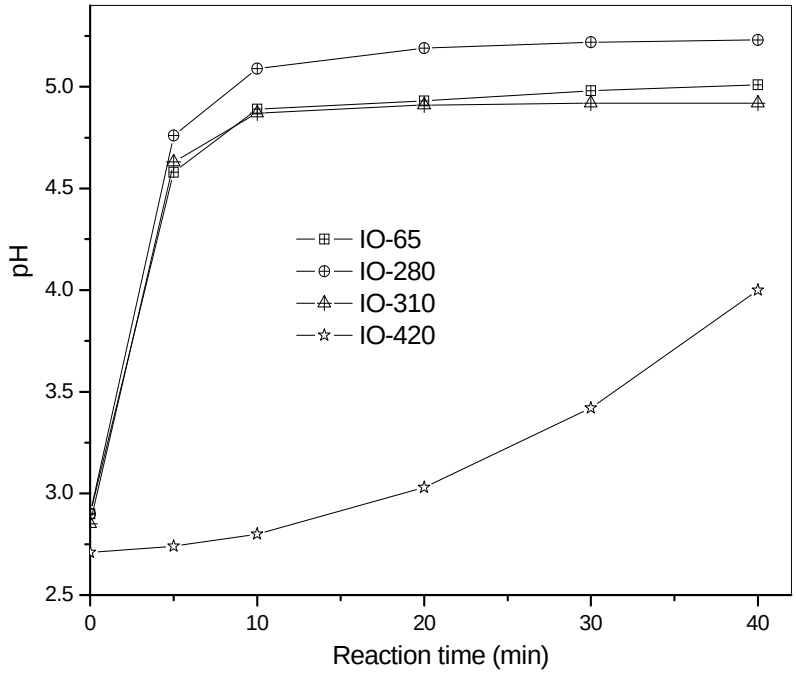
pH
5.0
4.5
4.0
3.5
3.0
2.5
0
10
20
30
40
Reaction time (min)
IO-65
IO-280
IO-310
IO-420

Fig. 8

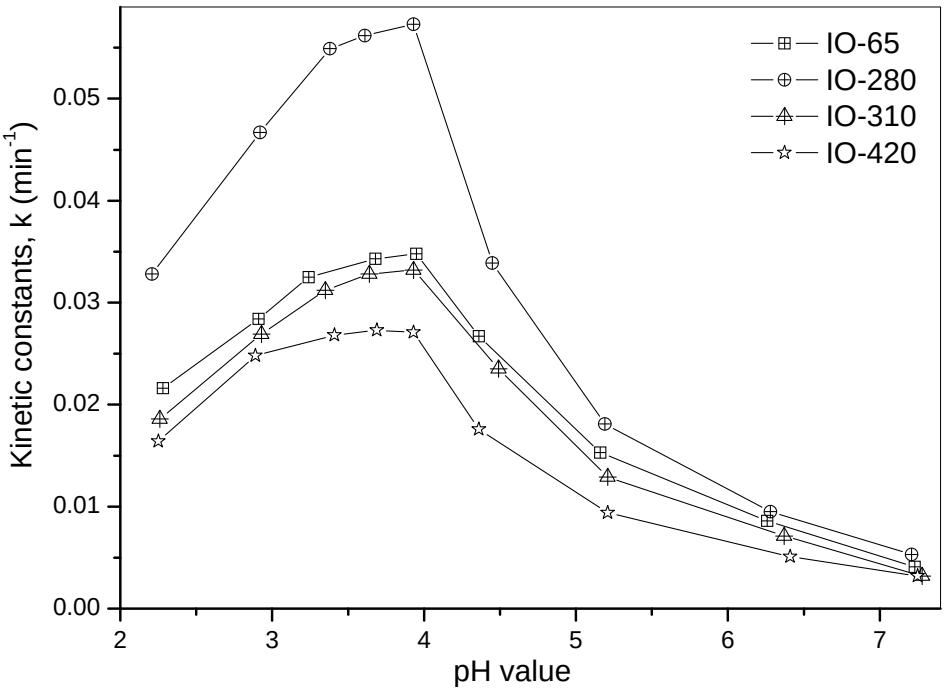
IO-65
IO-280
IO-310
IO-420
Kinetic constants, k (min-1)
0.00
0.01
0.02
0.03
0.04
0.05
2
3
4
5
6
7
pH value

505
506
507 FIG. 9
508
509

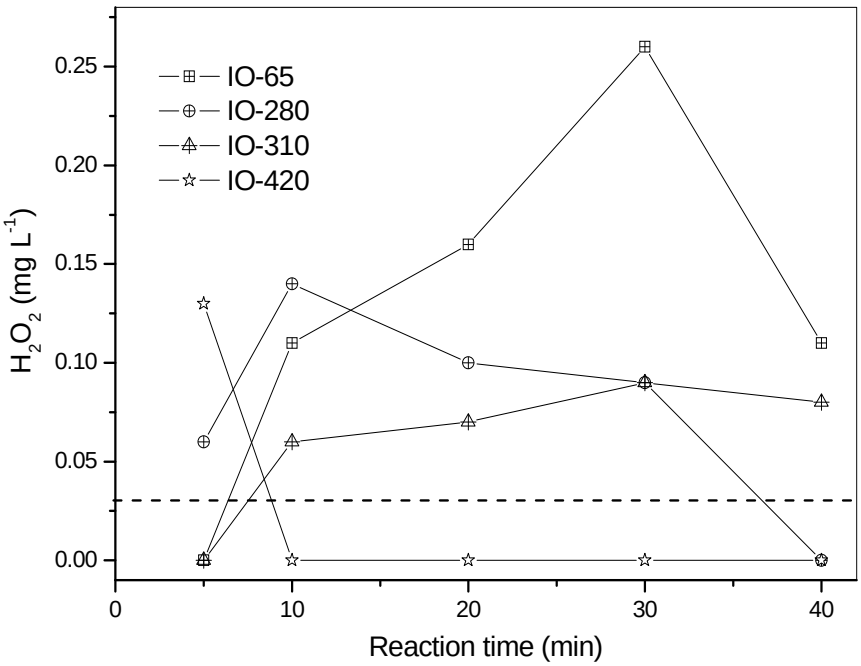

510
511
512
513
514

FIG. 10

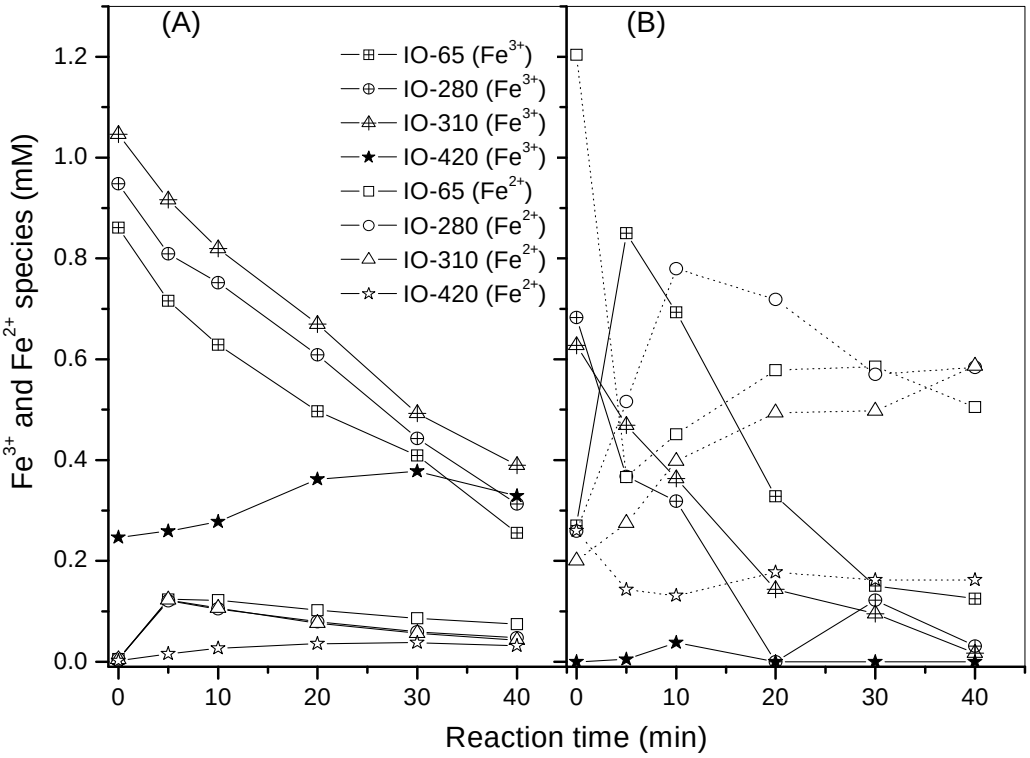
(A)
(B)
IO-65 (Fe3+)
IO-280 (Fe3+)
IO-310 (Fe3+)
IO-420 (Fe3+)
IO-65 (Fe2+)
IO-280 (Fe2+)
IO-310 (Fe2+)
IO-420 (Fe2+)
Fe3+ and Fe2+ species (mM)
Reaction time (min)
0.0
0.2
0.4
0.6
0.8
1.0
1.2
0
10
20
30
40